Atomization of Dilute Polyisobutylene/Mineral Oil Solutions

Joseph M. Smolinski, Esin Gulari, and Charles W. Manke
Dept. of Chemical Engineering, Wayne State University, Detroit, MI 48202

Atomization experiments, motivated by the need to suppress misting of machining oils, were conducted on dilute solutions of polyisobutylene (PIB) in mineral oil using a coaxial air blast atomizer and an optical (Fraunhofer diffraction) particle sizer. Polymer concentrations (0.1 to 1.0 kg/m^3) and molecular weight (1.0 to 2.2 million) were varied to determine their effects on aerosol drop-size distributions. The pure oil and PIB – oil solutions were atomized at air/liquid mass ratios near 10 and atomizing air velocities of 150 – 270 m/s, producing droplet-size distributions with mass mean diameters (MMD) in the range of 7 – 15 μm for the pure oil. Under identical atomization conditions, the MMDs of PIB solutions were 20 – 200% higher than pure oil. These observed increases in MMD correspond to significant reductions in the fraction of droplets falling below 5 μm in diameter that constitute the misting problem in industrial machining applications. Observed effects of PIB on atomization are ascribed to the viscoelastic properties of PIB – oil solutions as characterized by the elongational viscosity η_E. This relationship is examined by correlating the change in MMD caused by PIB addition with the stress-dependent elongational viscosity of PIB – oil solutions as predicted by the FENE-P dumbbell kinetic theory. The increase in MMD due to PIB varies linearly with the predicted η_E at constant atomization tensile stress.

Introduction

Our work is motivated by the need to suppress misting of machining fluids that are used in a variety of common industrial metalworking operations to lubricate and cool both machining tools and working surfaces. Most metalworking operations are performed on open floors in component plants, and the formation of machining fluid mist, that is, fine liquid droplets, due to breakup of liquid films and jets under impact or shear conditions has become an increased concern. A major health hazard is presented by mist drops under 5 μm in diameter, which are easily suspended in air and migrate throughout the plant. Substantial worker exposure to machining fluids may occur via inhalation of aerosol-laden air. The usual approach for minimizing exposure to aerosols from machining fluids is to provide enclosures and exhaust systems equipped with filters. These installations are in place in most modern plants, but they are not fully effective. Small drops in the micron-size range may also present a serious fire hazard. In the presence of a spark from a broken tool or simple frictional heating fine mist is easily ignited and the resulting flame travels throughout the venting ducts, causing substantial damage and expensive operational downtime. Approximately 20% of all machining fluids are straight mineral oils, with the remaining fraction being water-soluble oils or emulsions. Straight oils produce especially serious misting problems because they atomize very easily and produce aerosols that do not dissipate by evaporation. Unfortunately, high-quality surface finishes can often be achieved only with straight oil machining fluids, and at present they cannot be eliminated from many industrial operations. We examine a rheological mechanism for mist control by adding high molecular weight polyisobutylene (PIB) to straight mineral oils.

The ability of small amounts of dissolved polymer to suppress misting of liquids has been known for some time. In recent years, attempts have been made to reduce aerosol formation in a variety of operations by this means, particularly in the case of polymer antimisting additives for jet fuels (Chao et al., 1984; Peng and Landel, 1983; Hoyt et al., 1980). In the atomization experiments of Chao et al., dilute solutions of high molecular weight PIBs in jet fuel produced coarser spray

textures than pure jet fuel, and corresponding increases in the required ignition energies of the jet fuel sprays were observed when PIB was present. Antimisting action of the PIB–jet fuel solutions correlated with the elongational viscosity of the solutions, as characterized by ductless siphon measurements (Chao and Williams, 1983). This study echoed the findings of earlier work by Hoyt et al., in which several drag-reducing polymers, including PIB, reduced mist formation with kerosene. The success of these studies, as well as the chemical similarity of jet fuel (kerosene) and mineral oil, suggest that high molecular weight PIB may be an excellent polymeric antimisting additive for mineral-oil machining fluids.

In what follows, we report the results of a series of atomization experiments conducted to determine the effectiveness of PIB as an antimisting additive for mineral oils, and to evaluate the effects of PIB concentration and molecular weight on antimisting activity. Earlier antimisting studies with jet fuels (Chao et al., 1984; Chao and Williams, 1983; Peng and Landel, 1983; Hoyt et al., 1980) and a more recent study by Ferguson et al. (1992) on the atomization of aqueous polymer solutions all suggest that the atomization behavior of dilute polymer solutions is related to the elasticity of these liquids under the stress of atomization. Here, as in the study by Chao et al., we investigate the link between antimisting effectiveness and the elongational viscosity contributed by the polymer solutes. Since direct measurements of the elongational viscosity of polymer solutions are difficult, with different experimental techniques yielding widely varying results (Walters, 1992; Sridhar, 1990), our approach employs a simple molecular theory, the FENE-P dumbbell model (finitely extensible nonlinear elastic), to estimate elongational viscosity using measured values for the main relaxation time and contour length of the polymer molecules.

Experimental Studies

Materials

Four commercially available molecular weight grades of PIB, Vistanex L-80, L-100, L-120 and L-140 were obtained from Exxon. Molecular weight evaluations of each grade were performed by gel permeation chromatography (GPC) in toluene at 40°C and referenced to polystyrene standards in toluene. The weight-average molecular weights, used in all calculations here ranged from 1 to 2.2 million (Table 1).

Two viscosity grades of mineral oil were tested, and their properties are listed in Table 1. Both grades are used extensively in metal machining operations. Oil A was used for the majority of the testing, and oil B was used to examine the effects of varying solvent viscosity and intrinsic viscosity for a particular PIB solute.

Table 1. Material Properties

Polyisobutylenes Grade	M_W	M_N	M_W/M_N
L-80	1,020,000	430,000	2.37
L-100	1,350,000	640,000	2.11
L-120	1,700,000	830,000	2.05
L-140	2,200,000	1,070,000	2.06
Mineral Oils (measured at 23°C)			
Grade	**η (Pa·s)**	**σ (N/m)**	**ρ (kg/m^3)**
Oil A	0.020	0.028	820
Oil B	0.0058	0.028	820

The preparation of PIB–mineral-oil solution was begun by dissolving solid PIB in toluene at a concentration of 200 kg/m^3. Toluene was used in this step to facilitate the initial dissolution of PIB; subsequent dilutions, described below, yield solutions in which toluene is a minor component (< 1.5 wt. %) that does not affect the physical properties. The concentrated toluene–PIB solutions were then diluted with mineral oil to produce stock oil–PIB solutions of 20 kg/m^3. These stock solutions were allowed to rest for several weeks to ensure the complete dissolution of the polymer. To avoid any possible mechanical degradation of polymer molecular weight, mechanical agitation was not used in these steps. These oil–PIB stock solutions were further diluted with oil to yield the required PIB concentrations for atomization and rheological testing.

Solutions with PIB concentrations up to 1.0 kg/m^3 were examined in the atomization tests. At these concentrations, the surface tension and density of the mineral oils are not affected significantly by the addition of PIB. The viscosity increases moderately with the addition of PIB over the same concentration range (approximately a 16% increase in viscosity for 1.0 kg/m^3 L-80 in oil A). From intrinsic viscosity $[\eta]$ measurements, see Appendix B, we find that the largest $c[\eta]$ value of the atomized solutions is $c[\eta] = 0.16$ for L-80 at 1 kg/m^3, indicating that the solutions are in the dilute regime far below the value $c[\eta] = 1$ that corresponds to coil overlap and the onset of entanglements. Within this concentration range, the shear viscosity and other concentration-dependent rheological properties such as the complex viscosity components η' and η'', exhibit a linear dependence on concentration (Smolinski, 1994).

Atomization apparatus

Aerosol formation experiments used an "air blast" atomizer of coaxial design (Figure 1). Liquid is supplied to the atomizer tip through the center tube (ID 0.0011 m) by a syringe pump at constant flow rates up to 0.0084 L/min. Compressed air is supplied through the annulus between the OD (0.0013 m) of the inner tube and the ID (0.0021 m) of the

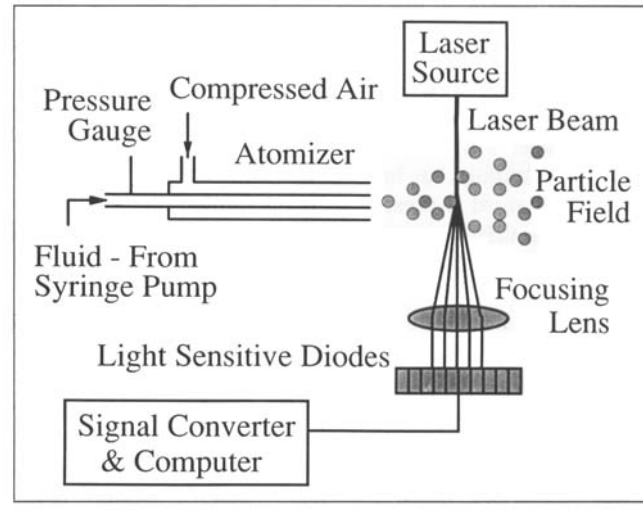

Figure 1. Atomizer and particle sizer.

Table 2. Parametric Range of Atomization Experiments

Air Flow Rates	
Volumetric-flow rate	$1.7\text{–}5.8\times10^{-4}$ m^3/s
Mass-flow rate	$2.2\text{–}7.5\times10^{-4}$ kg/s
Average nozzle velocity	80–270 m/s
Oil Flow Rates	
Volumetric-flow rate	5.5×10^{-8} m^3/s
Mass-flow rate	4.51×10^{-5} kg/s
Average nozzle velocity	0.06 m/s

outer tube. Atomization parameters are given in Table 2. Under these conditions, low Reynolds numbers ($N_{Re} < 10$) prevail for liquid flow in the supply tube, and the air flow is highly turbulent with $70\times10^3 < N_{Re} < 250\times10^3$. The liquid flow rate was varied only in preliminary experiments to establish the dependence of mass mean diameter (MMD) on the air–liquid mass ratio. All subsequent atomization experiments were performed at a fixed liquid flow rate of 0.0033 L/min, which corresponds to a shear rate of 420 s^{-1} in the supply tube. Direct measurements of the kinematic conditions for liquid atomization at the nozzle tip were not possible, and the best characterization comes from the elongational stress measurements described below. However, in utilizing the FENE-P model, strain rates are calculated as an intermediate step in predicting the stress-dependent elongational viscosity. For the range of conditions encountered here, the corresponding range of nozzle-tip strain rates inferred through the model was 300 to 3,000 s^{-1} for the PIB–oil solutions tested.

The coaxial atomizer design was selected for its simple, symmetric geometry, which facilitates evaluation of the average extensional stresses encountered at the nozzle tip during atomization. The measurement of extensional stress in the liquid is accomplished by the use of a pressure gauge placed in the liquid supply line upstream of the atomizer tip. For steady-state flow of liquid, a force balance gives the total tensile stress $\langle\Pi_{ZZ}\rangle_G$ at the position of the pressure gauge as

$$\langle\Pi_{ZZ}\rangle_G = \langle\Pi_{ZZ}\rangle_T + 4\left(\frac{L}{d_0}\right)\tau_W, \tag{1}$$

where $\langle\Pi_{ZZ}\rangle_T$ is the average ZZ component of the total stress tensor at the atomizer tip, with Z denoting the axial direction, and τ_w is the wall shear stress produced by the flow in the liquid tube. The ID of the liquid tube is d_0, and L is the distance between the pressure gauge and the tip. Although viscoelastic fluids can develop first and second normal stress differences under shear flow (Bird et al., 1987a), we demonstrate in Appendix A that such normal stress differences are negligible for the low polymer concentrations and low Weissenberg numbers that pertain to liquid flow in the supply tube for our experiments. Neglecting both first and second normal stress differences during flow in the liquid tube, we obtain $\langle\Pi_{ZZ}\rangle_G = P_G$ and $\langle\Pi_{ZZ}\rangle_T^{\text{Air off}} = P_{\text{atm}}$ for the liquid exiting at the nozzle tip in the absence of atomizer air flow. In the presence of an atomizer air flow, $\langle\Pi_{ZZ}\rangle_T < P_{\text{atm}}$, due to the presence of a tensile stress within the liquid. For the same liquid flowing at the same flow rate, the difference in the pressure gauge reading, measured with and without air flow, gives

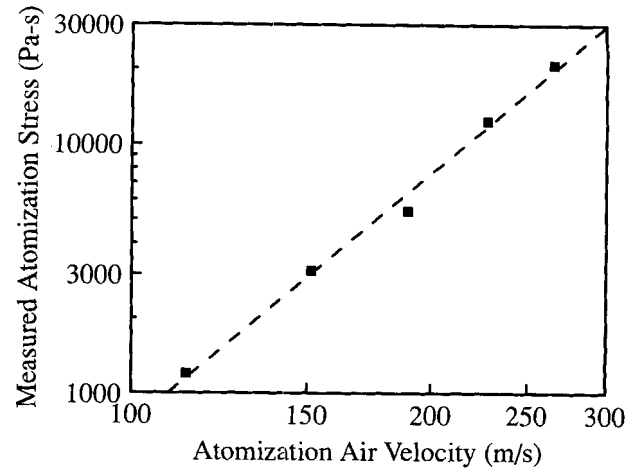

Figure 2. Variation of extensional stress, $-(P_G^{\text{Air on}} - P_G^{\text{Air off}})$, with atomization air velocity.

$$(P_G^{\text{Air on}} - P_G^{\text{Air off}}) = \langle\Pi_{ZZ}\rangle_T^{\text{Air on}} - P_{\text{atm}}. \tag{2}$$

This stress measurement characterizes the magnitude of the extensional stress encountered by the liquid during atomization. For our atomizer, this was found to vary with air velocity as shown in Figure 2. The measured extensional stress did not vary with liquid flow rate, and at identical air velocity it was found to be the same for all liquids tested, including the viscoelastic oil–PIB solutions.

The aerosol generated by the atomizer is directed into a long, 0.127-m-wide plexiglass duct of square cross section. The aerosol is carried through the duct by a secondary air stream introduced behind the atomizer. Two small openings placed on either side of the duct, at a distance of 0.038 m from the tip of the atomizer, provide a clear optical path for particle sizing. Containment of the aerosols is accomplished by holding the duct pressure slightly below ambient, with suction provided by a small blower at the exhaust end of the duct.

Aerosol sizing is performed with a Malvern 2600 Particle Sizer, which analyzes the Fraunhofer diffraction pattern formed when a laser beam traverses the aerosol field (Swithenbank et al., 1977). A 2-mm-diameter collimated He–Ne laser beam passes through the openings in the duct and intercepts the center line of the spray cone at a distance of 0.038 m from the atomizer tip. The forward scattered light is collected by a focusing lens and directed onto an optical detector consisting of 32 light-sensitive diodes. The diodes are semicircular in shape and logarithmically spaced in the detection plane. The light-energy distribution incident on each diode element originates primarily from the forward scattering of a characteristic drop size. The unobstructed fraction of the light passing through the aerosol field is focused onto the central diode element. Scattered light from larger aerosol particles is focused onto the inner diodes, while the scattered light from smaller aerosols is focused on the outer diodes. Thus, the scattered light energy distribution detected by the geometrically defined diode array detector contains the aerosol size information. Particles as small as 2 μm can be accurately sized by this means. The aerosol size distribution is computed from the light-energy distribution by assuming a Rosin-Rammler distribution and minimizing the de-

viation between the computed and measured light intensities in order to obtain optimum values of the Rosin-Rammler distribution parameters X and N, such that

$$R = 1 - \exp\left[-\left(\frac{\chi}{X}\right)^N\right], \tag{3}$$

where R is the mass fraction of particles below diameter χ.

The weight distribution function is $W(\chi) = dR/d\chi$. The MMD, which is used later to characterize aerosols, can be expressed in terms of the Rosin-Rammler parameters X and N by the following equation:

$$\text{MMD} = X[\ln(2)]^{1/N}. \tag{4}$$

The Sauter mean diameter (SMD), used in Eq. 6, can also be expressed in terms of these parameters as

$$\text{SMD} = \frac{X}{\Gamma[(2-1/N)(1-1/N)]}. \tag{5}$$

Rheological instrumentation

Rheological characterizations of the oil–PIB solutions were conducted on a Weissenberg Rheogoniometer (model R21) fitted with 0.075-m parallel platens at a gap setting of 250 μm. Steady shear measurements were conducted at shear rates ranging from 1 to 20 s^{-1}, while oscillatory shear flow testing was performed over a frequency range of 1 to 45 Hz. Shear viscosity measurements were performed on oil–PIB solutions with concentrations in the dilute regime up to 1.0 kg/m^3 to determine the intrinsic viscosities of the PIB solutes in the mineral oils.

Oscillatory shear flow measurements were performed to evaluate the storage modulus G' as a function of frequency for each oil–PIB system. Oscillatory measurements at frequencies between 20 and 30 Hz were subject to vibrational interference, leaving a gap in the storage modulus data in this region. The dominant relaxation time for each oil–PIB system was evaluated from the storage modulus measurements (Appendix B). These were measured at somewhat higher PIB concentrations, up to 8 kg/m^3, to provide stronger torsion signals. Even at these higher concentrations, however, G' was found to vary linearly with concentration.

Results and Discussion

Atomization results

The atomization behavior of the two pure mineral oils was first examined to establish baseline particle size distributions without additives, and to evaluate the effects of atomization air velocity and the air-to-liquid mass ratio (ALR) on the resulting particle size distribution. As expected, atomization air velocity and ALR had significant effects on the particle size distribution. The average drop size (MMD) decreases with increasing air velocity and ALR, as shown in Figure 3 for oil A at various air velocities. In addition to decreasing the MMD, increases in atomization air velocity also produce narrowing of the drop-size distributions (Figure 4). Increases in the ALR cause slight decreases in the MMD, but have little

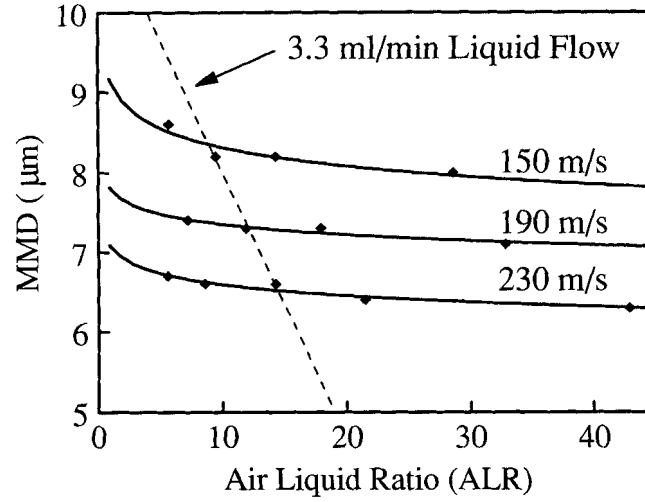

Figure 3. Effects of air velocity and air–liquid ratio on the atomization behavior of oil A.

effect on the widths of the drop-size distributions. These observed effects of air velocity and ALR are consistent with previous studies on the atomization of Newtonian fluids (Nukiyama and Tanasawa, 1939; Lefebvre, 1980).

For high ALR (ALR > 5), the effect of ALR on the drop-size distribution is minor compared to the effect of air velocity, thus the effects of ALR on atomization behavior were not investigated further in this work. All subsequent atomization experiments were conducted at a fixed liquid flow rate of 3.3 mL/min. Holding the liquid flow rate constant caused the ALR to vary with the atomization air velocity, but the effect of this variation on the average drop size is minor in the region tested, as shown in Figure 3, where the dashed line indicates constant liquid flow conditions.

The particle size distributions produced by our atomizer did not vary noticeably with liquid viscosity in tests performed on the pure oils. Oil A and oil B, which differ in viscosity by more than a factor of 3, behaved identically during atomization over the entire range of conditions examined (for example, compare the oil A and oil B curves in Figure

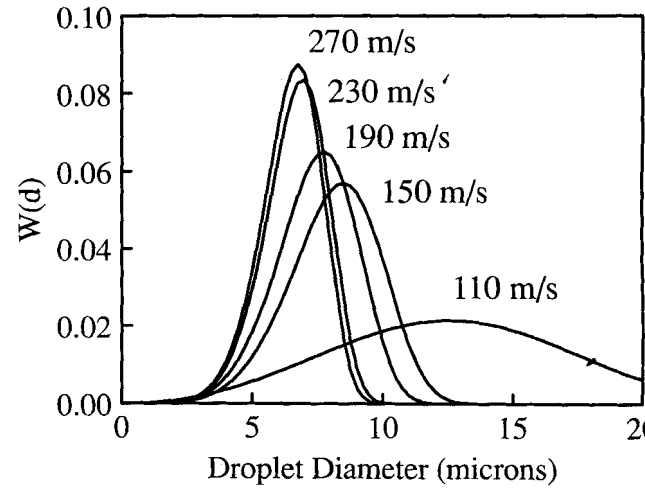

Figure 4. Effects of air velocity on drop size distribution atomization produced by oil A.

10, which is discussed below). For these low-viscosity Newtonian liquids, the effects of viscosity were apparently overwhelmed by the relatively large capillary and inertial forces produced by the small nozzle size and the high air velocities characteristic of our atomizer. However, further atomization tests conducted with Newtonian liquids of viscosities two orders of magnitude greater than the mineral oils did begin to show an increase of MMD with viscosity.

The addition of PIB to the mineral oils produced viscoelastic solutions, as indicated by the G' measurements discussed in Appendix B. These viscoelastic solutions exhibited substantially larger MMDs under atomization than the Newtonian mineral oils. The amount of increase in the average drop size is influenced by the PIB concentration, PIB molecular weight, and solvent viscosity of the atomized solution. As expected, the solutions of highest concentrations, highest molecular weights, and highest oil viscosity exhibit the greatest increases in aerosol drop size relative to pure oil atomized at the same conditions. In addition to increasing the MMD, PIB additions also broaden the drop-size distribution.

The effect of PIB concentration on aerosol drop size is shown in Figures 5 and 6, where the Rosin-Rammler distributions are shown for solutions of various concentrations of L-80 atomized at air velocities of 150 and 230 m/s. PIB concentrations as low as 0.10 kg/m^3 produce a substantial increase in the average drop size. Higher concentrations of PIB (0.5 and 1.0 kg/m^3) further increase average drop size and produce very broad drop-size distributions, similar to those displayed by pure oil at lower air velocities, as in Figure 4.

PIB is most effective at increasing the average drop size, relative to pure oil, at the lower atomization air velocities (Figure 5), where the addition of PIB typically produces extremely large increases in drop size. In several cases, the MMD increased 200 to 300% relative to pure oil. At higher air velocities (Figure 6) the effects of PIB additions on drop size are less pronounced, though still significant.

The increases in overall drop size of the aerosols due to PIB additions are accompanied by a significant decrease in the fraction of small drops (≈ 8 μm or less) within the aerosols. This can be seen in Figure 7, where a comparison of

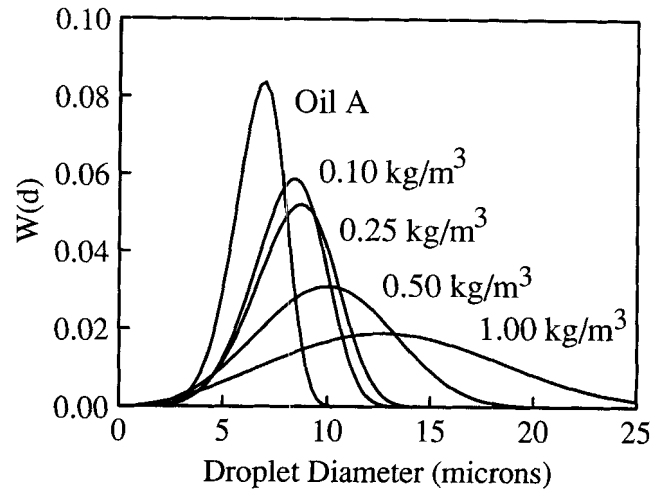

Figure 6. Effects of PIB concentration on the atomization behavior of oil A: atomization velocity, 230 m/s; PIB grade, L-80.

the cumulative weight fraction, as a function of particle size, is shown for oil A and two typical oil–PIB solutions. This figure illustrates the practical benefits of PIB as an antimisting additive, because drops in this size range remain airborne for extended periods of time and create most of the *oil mist* problems encountered in metalworking facilities.

Like the effect of increasing polymer concentration, increasing the molecular weight of the PIB solute, through use of higher grades of the Vistanex "L" series (see Table 1), produces increasingly larger drop sizes in the atomized liquid. Figure 8 shows that this trend is clearly prevalent at relatively low atomizer air velocities (150 m/s). The increase of MMD with PIB molecular weight is sharply diminished at high air velocities, however. Figure 9, displaying data taken at 230 m/s atomizer air velocity, shows very little difference between the drop-size distributions for L-80 and L-140, though the drop sizes for all the polymer solutions are distinctly larger than those for pure oil.

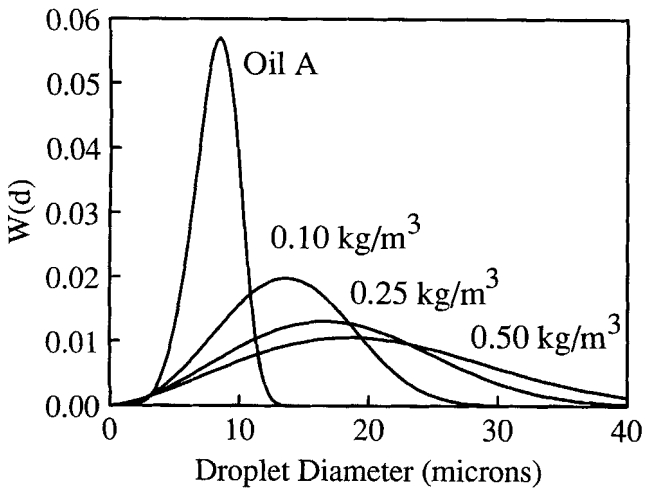

Figure 5. Effects of PIB concentration on the atomization behavior of oil A: atomization velocity, 150 m/s; PIB grade, L-80.

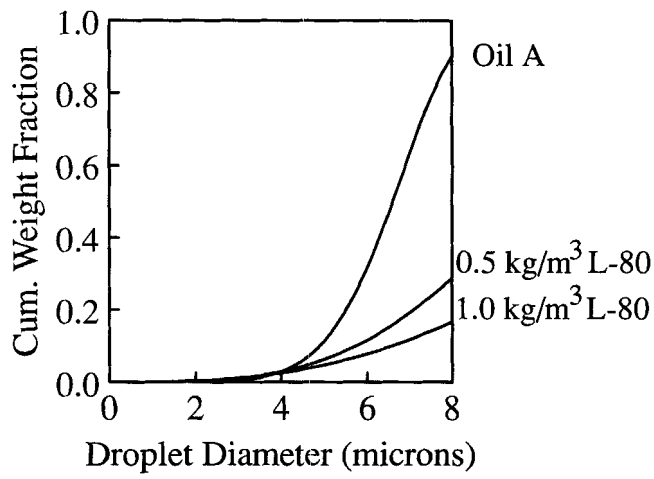

Figure 7. Cumulative weight fraction as a function of particle size between oil A and oil/L-80 solutions: atomization velocity, 230 m/s.

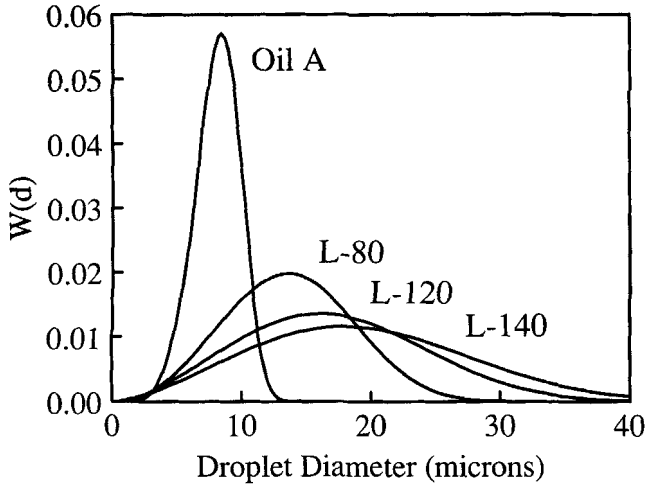

Figure 8. Effects of PIB molecular weight on the atomization behavior of oil A: atomization velocity, 150 m/s; PIB concentration, 0.10 kg/m^3.

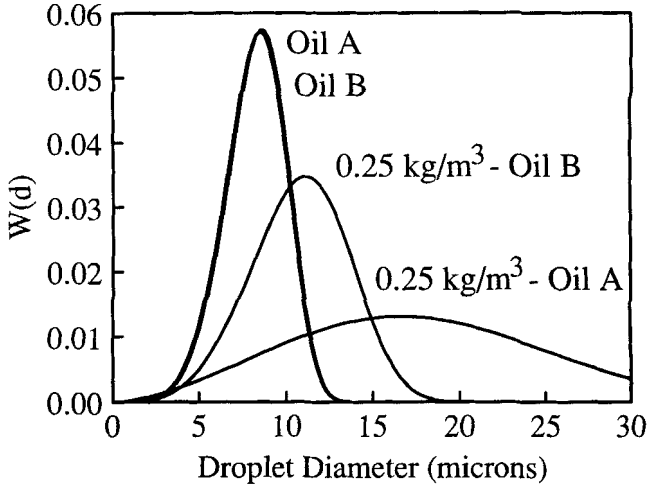

Figure 10. Oil viscosity effects on atomization of oil/PIB solutions: atomization velocity, 150 m/s; PIB grade, L-80; PIB concentration, 0.25 kg/m^3.

Although oil viscosity has no effect on the atomization behavior of pure oil A and oil B in our atomizer, solvent viscosity does exert a significant influence on the behavior of mineral-oil–PIB solutions. This can be seen in Figure 10, where the Rosin-Rammler distributions are shown for 0.25 kg/m^3 of L-80 in each of the oils at an air velocity of 150 m/s. The same concentration of L-80 produces larger drop-size distributions when used with the more viscous of the two oils examined. In comparing the rheological properties of L-80 in oil A and oil B, we note that both oils are good solvents for PIB, and that oil B is a better solvent for L-80 than oil A. This is evident from the mechanical relaxation time measurements and the intrinsic viscosities presented in Appendix B, where $[\eta]_B > [\eta]_A$, and $\lambda_B \eta_{S(A)}/\lambda_A \eta_{S(B)} > 1$, which both indicate a larger coil size for L-80 in oil B. Nevertheless, we believe that the difference in the L-80 atomization curves shown in Figure 10 are due almost entirely to the effect of solvent viscosity, and that solvent power has very little influence. The reason for this interpretation is that the high-strain-rate η_E varies with parameters that depend on solvent viscosity but not solvent power. We give a more complete discussion of this point in a later section, and also show that η_E is the dominant rheological parameter controlling the droplet-size distribution in our experiments.

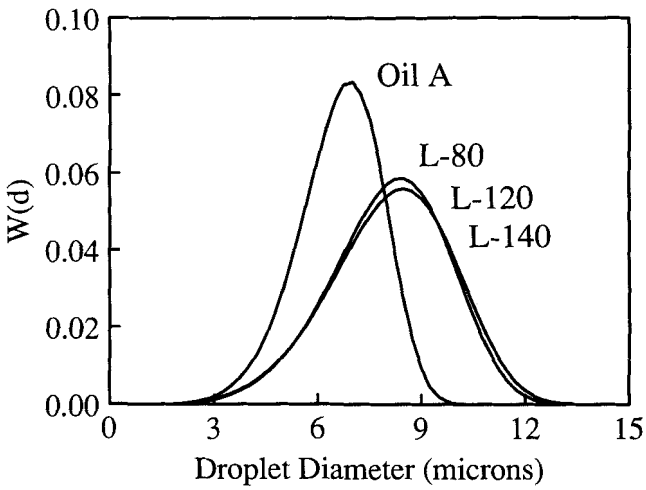

Figure 9. Effects of PIB molecular weight on the atomization behavior of oil A: atomization velocity, 230 m/s; PIB concentration, 0.10 kg/m^3.

The L-120 and L-40 curves appear to be identical.

Our atomization results are in general agreement with the previous studies of Chao et al. (1984) and Hoyt et al. (1980), in which higher concentrations and molecular weights of PIB were found to be more effective at mist suppression. Both of these studies showed L-140 to be markedly superior to L-80 at mist suppression. Chao et al. found L-140 at low concentrations to be as effective at mist suppression (measured in their study by ignition energies) as L-80 at concentrations an order of magnitude higher, even though the two polymers differ in molecular weight by only a factor of 2. Since the work of Chao et al. was conducted at air atomization velocities lower than those used in our study, this result is consistent with our finding that increasing PIB molecular weight is a highly effective means of enhancing mist suppression at low atomization air velocities.

Figures 5–9 show that the antimisting effectiveness of PIB depends on kinematic conditions (atomizer air velocity), as well as polymer concentration, polymer molecular weight, and solvent viscosity, and that dependence of the drop-size distribution on these variables is not simple. For example, Figures 5 and 8 show that increasing either polymer concentration or molecular weight improves the ability of the solution to resist mist formation at low atomization air velocities. At higher atomization air velocities, Figures 6 and 9, antimisting effectiveness increases with PIB concentration, but drop sizes are relatively insensitive to PIB molecular weight. These complexities are to be expected because the high deformation rates that attend atomization can easily drive viscoelastic liquids such as our PIB solutions into regimes of nonlinear rheological behavior. In the following sections, we link the observed atomization behavior to the nonlinear rheological properties of the PIB solutions by employing a molecular rheological theory for dilute polymer solutions.

Rheological correlation of atomization results

Atomization of viscoelastic liquids is not well understood, and there are no fluid mechanical models available to describe the breakup of these liquids under atomization. Therefore our efforts are directed toward the development of correlations of the drop sizes produced by atomization of the PIB–oil solutions with the rheological properties of those solutions. However, some features of the breakup mechanism may be similar to capillary breakup of viscoelastic liquid jets, where extensive modeling has been done (Goren and Gottlieb, 1982; Bechtel et al., 1987; Bousfield et al., 1986). These models predict that an initial axial tension within a viscoelastic liquid jet will stabilize the jet against capillary breakup, producing larger drops upon breakup than an equivalent Newtonian liquid jet. A reduction in the number of satellite droplets formed, due to an initial elastic stress, is also predicted. While these jet breakup predictions qualitatively describe the observed antimisting behavior of viscoelastic fluids, the models apply only to primary capillary breakup of a liquid jet, and cannot describe the random tertiary liquid breakup that is characteristic of fluid atomization.

Research on the atomization of Newtonian fluids has been directed primarily toward development of empirical equations that predict the average drop size of an aerosol under given conditions. These empirical equations vary widely in their representation of the effects of atomization parameters on drop-size distributions, depending on the particular atomizer design and fluid tested. However, most of these equations express the average drop size as the sum of a term representing inertial forces and a term representing viscous forces, as illustrated by the following empirical equation developed by Rizk and Lefebvre (1984):

$$\frac{\mathrm{SMD}}{d_0} = 0.48\underbrace{\left(\frac{\sigma}{\rho_A V_R^2 d_0}\right)^{0.4}\left(1+\frac{1}{\mathrm{ALR}}\right)^{0.4}}_{\text{inertial term}} + 0.15\underbrace{\left(\frac{\eta_L^2}{\sigma\rho_L d_0}\right)^{0.5}\left(1+\frac{1}{\mathrm{ALR}}\right)}_{\text{viscous term}}. \quad (6)$$

The general form of empirical equations such as Eq. 6, and not the specific mathematical structure of the individual terms, is of interest here. In interpreting our atomization data for PIB–oil solutions, we assume that the mean drop size for an atomized viscoelastic liquid can also be expressed as the sum of separable inertial and viscous terms. Under this assumption, the inertial-force terms, which are strong functions of the air velocity and atomizer geometry, are the same for both the pure mineral oil and the oil–PIB solutions under identical air and liquid flow rates, and any observed difference in the average drop size can be attributed entirely to a difference in the viscous terms. The recent work on the atomization of elastic fluids by Ferguson (Ferguson et al., 1992), and the findings of the earlier antimisting studies (Chao et al., 1984; Hoyt et al., 1980) all suggest that the elongational viscosity of viscoelastic solutions characterizes the viscous forces that develop during atomization. While the viscous force term for the pure mineral oils was found to be negligible for our atomizer design and conditions, the high elongational viscosities of the oil–PIB solutions produce significant viscous forces during the atomization of these solutions. Thus the observed increase in average drop size for the oil–PIB solutions is expected to depend directly on the elongational viscosities of the solutions. The relationship between aerosol drop size and elongational viscosity is examined below by correlating the change in average drop size produced at various stress levels, and for various PIB concentrations and molecular weights, to the elongational viscosity predicted by the FENE-P model, a simple molecular rheological theory.

Prediction of elongational viscosities

The elongational viscosities of the oil–PIB solutions are estimated by employing the FENE-P dumbbell model with a preaveraged closure approximation (see Bird et al., 1987b) for dilute polymer solutions. This simple model represents a polymer molecule in solution as an assembly of two frictional beads, which experience hydrodynamic drag forces from the surrounding solvent, connected by a nonlinear spring that represents entropic forces along the polymer chain backbone. The FENE-P spring connector force F^C is

$$F^C = \frac{HQ}{1-\langle Q^2/Q_0^2\rangle}, \quad (7)$$

where H is the spring constant, Q is the vector connecting the beads of the dumbbell, and Q_0 is the maximum spring extension. As $|Q|$ approaches Q_0, under flow at high deformation rates, the contractile spring force F^C becomes infinite, thereby constraining the dumbbell to a finite maximum extensibility. Clearly, Q_0 is proportional to the contour length, and hence the molecular weight, of the polymer solute. These properties of the FENE-P model are incorporated in the model parameters

$$\lambda = \frac{\zeta}{4H} \quad (8)$$

and

$$b = \frac{HQ_0^2}{kT}, \quad (9)$$

where ζ is the bead friction factor.

The connection between molecular properties and macroscopic stresses for this type of model is described in detail by Bird et al. (1987b). Briefly, the dumbbell connector force law, Eq. 7, appears in force balance equations for the beads, which are combined with a conservation equation to form a "diffusion" equation governing the configurational properties of the model polymer molecules. Configurational moments of the diffusion equation are combined with an appropriate expression for the fluid stress, that is, the Kramers or Giesekus equations, to obtain the predicted elongational viscosity η_E of the polymer solution. Using Eq. 7 for the dumbbell connector force, Eq. 13.2-16 of Bird et al. (1987b) can be specialized for the case of steady-state uniaxial elongational flow and applied directly to obtain the configurational quantities needed for stress predictions:

$$\langle Q_X^2\rangle = \frac{kT}{H}\left[\frac{1}{1-\langle Q^2\rangle H/(bkT)} + \lambda\dot{\epsilon}\right]^{-1} \quad (10)$$

and

$$\langle Q_Z^2\rangle = \frac{kT}{H}\left[\frac{1}{1-\langle Q^2\rangle H/(bkT)} - 2\lambda\dot{\epsilon}\right]^{-1}. \quad (11)$$

The mean square length of the dumbbell $\langle Q^2\rangle$ is given by

$$\langle Q^2\rangle = 2\langle Q_X^2\rangle + \langle Q_Z^2\rangle, \quad (12)$$

which yields the strain-rate dependent $\langle Q^2\rangle$ as the positive, real root of a cubic equation when Eqs. 10 and 11 are substituted into Eq. 12. Equations 10 and 11 are also used in the Krammers equation for stress (Table 13.3-1 of Bird et al., 1987b) to obtain the extensional stress for steady-state elongational flow

$$\Pi_{ZZ} - \Pi_{XX} = -3\eta_S\dot{\epsilon} - 3nkT\lambda\dot{\epsilon} \times\left[\frac{1-\langle Q^2\rangle H/(bkT)}{\{1-2\lambda\dot{\epsilon}[1-\langle Q^2\rangle H/(bkT)]\}\{1+\lambda\dot{\epsilon}[1-\langle Q^2\rangle H/(bkT)]\}}\right]. \quad (13)$$

Equations 10–13 are employed in our analysis to estimate the strain rates $\dot{\epsilon}$ that would be prevalent in steady-state elongational flow at the values of extensional stress measured in our atomization experiments. These strain-rate values are then used to estimate the steady-state elongational viscosities that would correspond to the measured extensional stresses:

$$\eta_E = \frac{-(\Pi_{ZZ} - \Pi_{XX})}{\dot{\epsilon}}. \quad (14)$$

To model our oil–PIB solutions as solutions of FENE-P dumbbells, it was necessary to evaluate λ and b from measurements of solution rheological properties. The relaxation time λ for each solution was obtained from storage modulus measurements (Appendix B). The contour length Q_0 for each of the polymers was evaluated from the weight average molecular weight of the polymers as determined by gel permeation chromatography (GPC) and from the knowledge of the polymer structure; this calculation is also described in Appendix B. Two additional parameters, solvent viscosity η_s (measured) and the number concentration of polymer molecules in solution n (calculated from the mass concentration using M_w values obtained by GPC), are required to specify the stress–strain rate relationship, Eq. 13. Table 3 shows the values of the parameters used to describe each system. The parameter n (number of polymer molecules per unit volume), was the only value that changed with concentration. For the range of polymer concentrations and extensional stresses examined here, the polymer contribution to η_E was 10^2 to 10^3 times greater than the solvent contribution $3\eta_S$.

With these parameters, the FENE-P model was used to predict the elongational viscosity as a function of elongational stress for each oil–PIB solution of interest. High extensions of the PIB molecules (often in excess of 50% of contour length) were frequently predicted, particularly at low PIB concentrations or at high fluid stresses. These large molecular deformations illustrate the need for a nonlinear spring

Table 3. Model Parameters Required to Define Oil/PIB Solutions

System	λ (s)	b	η_s (Pa·s)
L-80 in oil A	0.00145	11,000	0.020
L-80 in oil B	0.00075	11,000	0.0058
L-100 in oil A	0.00168	14,700	0.020
L-120 in oil A	0.00215	18,600	0.020
L-140 in oil A	0.00265	23,700	0.020

such as the FENE-P force law, which ensures that chains cannot extend beyond a finite contour length. Under these conditions, the linear Hookean force law would predict unrealistically high elongational viscosities, as shown in Figure 11. At infinite strain rate, the limiting elongational viscosity predicted by the FENE-P model is

$$\eta_{E\infty} = 3\eta_S + \frac{1}{2}n\zeta Q_0^2. \quad (15)$$

Although the FENE-P model does not explicitly model solvent power effects, our earlier remarks concerning the relative importance of solvent viscosity and solvent power in governing atomization of polymer solutions can now be examined in light of the limiting high-strain-rate behavior of η_E. The chain contour length Q_0 and polymer number concentration n are independent of both viscosity and solvent power, whereas ζ is expected to depend directly on η_S. To at least a first approximation, Eq. 15 does not contain any terms that would change with solvent power. Thus we conclude that solvent viscosity plays the dominant role in differentiating the droplet size distributions for a given polymer dissolved in different solvents, such as the data shown in Figure 10.

Variation of atomized drop size with elongational viscosity

When elongational viscosities predicted by Eqs. 10–14 for the oil–PIB solutions at a given stress are correlated with

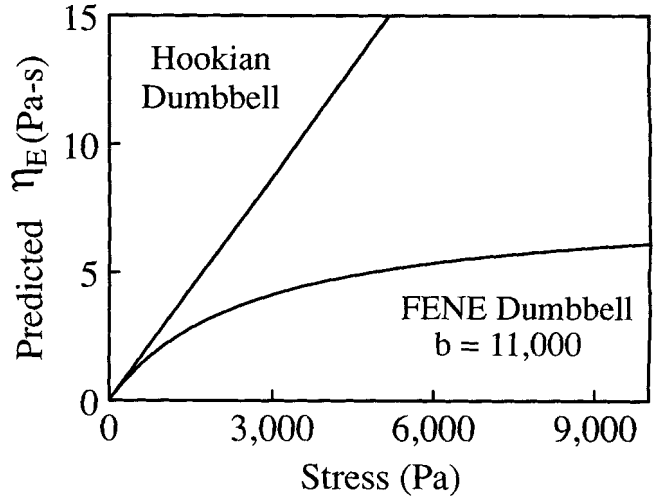

Figure 11. Elongational viscosities predicted by FENE-P and Hookean dumbbell models as a function of stress.

The parameters used for the case shown are $\lambda = 0.00145$ s, $\eta_s = 0.020$ Pa·s, and $n = 5.9\times10^{13}$ molecules/cm^3, which correspond to L-80 dissolved in oil A at 0.1 kg/m^3.

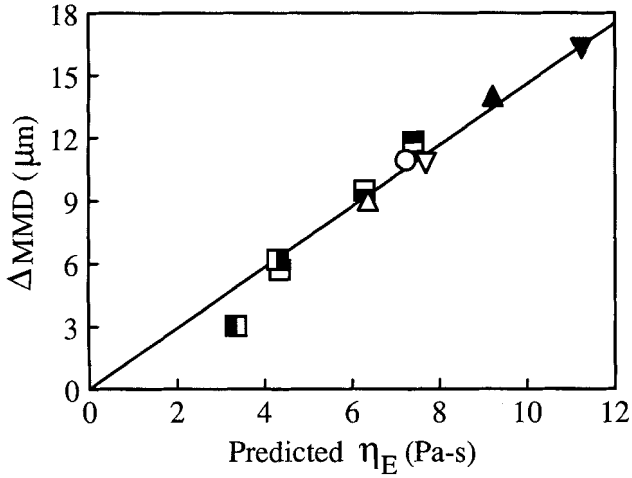

Figure 12. Correlation of predicted elongational viscosities with corresponding shifts in average drop size at a fluid stress of 3,100 Pa (150 m/s air velocity).

See Table 4 for definition of symbols.

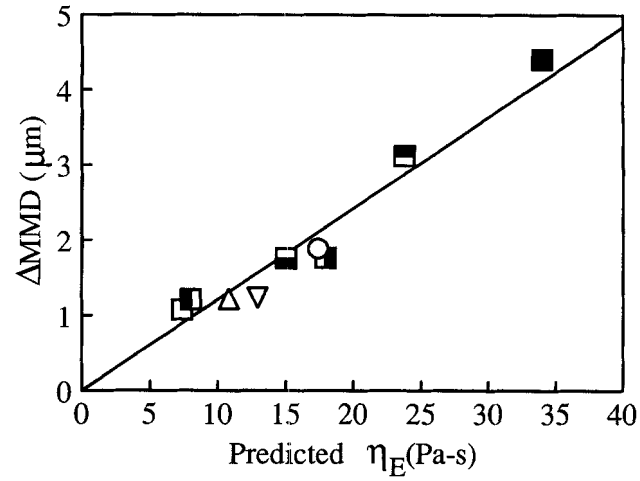

Figure 14. Correlation of predicted elongational viscosities with corresponding shifts in average drop size at a fluid stress of 20,800 Pa (270 m/s air velocity).

See Table 4 for definition of symbols.

ΔMMD, the increase in MMD relative to pure oil ($MMD_{oil-PIB} - MMD_{oil}$), one finds a strong linear relationship between the observed increase in average drop size and the elongational viscosity. Examples of this correlation are given in Figures 12–14 at various fluid stresses, with the legend for these figures given in Table 4. These results support the earlier supposition that elongational viscosity characterizes the viscous forces for viscoelastic fluids such as our oil–PIB solutions. The data presented in Figures 12–14 have been taken at various PIB concentrations, PIB molecular weights, and at different solvent viscosities (oil A and oil B). The excellent correlation of change in MMD with the predicted elongational viscosity indicates that the influences of these experimental variables are correctly represented in the η_E–stress relationship given by the FENE-P theory. Thus the seemingly complex dependence of atomization behavior on PIB concentration, PIB molecular weight, solvent viscosity, and atomization stress in our experiments is satisfactorily explained by a relatively simple rheological model.

The linear variation of ΔMMD with η_E shown in Figures 12–14 appears to confirm the linear variation of mean drop diameter with viscous force commonly given by empirical expressions such as Eq. 6. (Because Eq. 6 was developed for Newtonian fluids, for which $\eta_E = 3\eta$, it can be recast as a correlation of drop size with the magnitude of *tensile* stresses, consistent with the non-Newtonian results shown here.) However, examination of the slopes of the correlation lines in Figures 12–14 reveals that the slope $\partial\Delta MMD/\partial\eta_E$ decreases with extensional stress, as shown in Figure 15, rather than remaining nearly constant as Eq. 6 would suggest. (The variations of ALR in our experiments would produce a 20% change at most in the coefficient $1+1/ALR$ used in Eq. 6, which is much smaller than the decrease of $\partial\Delta MMD/\partial\eta_S$ with stress shown in Figure 15.) The reduction of the η_E-dependent antimisting effect with increasing extensional stress (increasing air velocity) explains why PIB additions are more effective at increasing aerosol drop size at low air velocities than at high air velocities, as observed earlier in our discussion of Figures

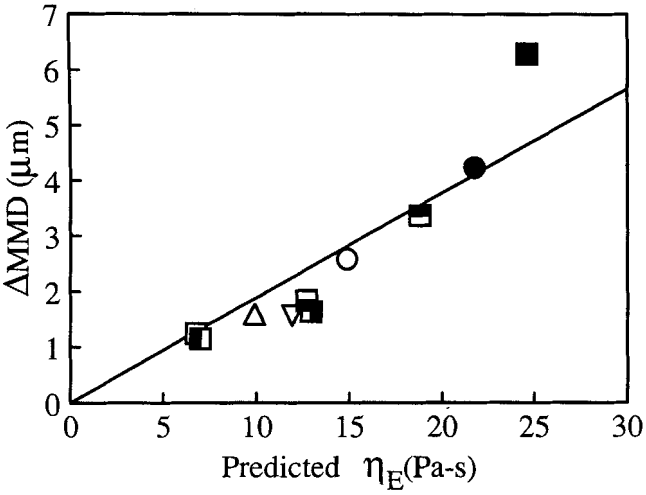

Figure 13. Correlation of predicted elongational viscosities with corresponding shifts in average drop size at a fluid stress of 12,400 Pa (230 m/s air velocity).

See Table 4 for definition of symbols.

Table 4. Legend for Figures 12 through 14

Polymer Grade	Conc. kg/m³	Oil Grade	Symbol
L-80	0.10	A	□
L-80	0.25	A	◒
L-80	0.50	A	◓
L-80	1.00	A	■
L-80	0.25	B	◧
L-80	1.00	B	◨
L-100	0.25	A	○
L-100	0.50	A	●
L-120	0.10	A	△
L-120	0.25	A	▲
L-140	0.10	A	▽
L-140	0.25	A	▼

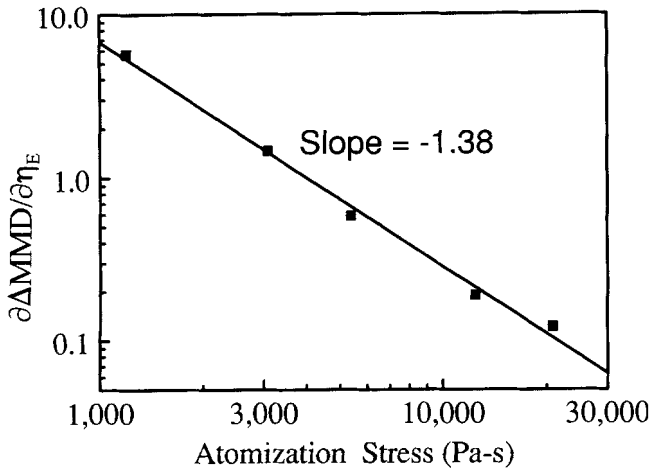

Figure 15. Dependence of $\partial\Delta MMD/\partial\eta_E$ on extensional stress.

5–9. Physically, this behavior can be explained by observing that the inertial forces associated with the atomizing air stream increase with V_A^2. At strain rates in the vicinity of $\dot{\epsilon} = 1/2\lambda$, molecular theories such as the FENE-P model predict a regime of strain-rate thickening η_E that would allow viscoelastic (tensile) forces to increase more than linearly with V_A. At high strain rates, however, finite polymer chain contour lengths impose an upper limiting value for η_E, and ultimately the viscous resistance can increase only linearly with V_A. Therefore at sufficiently high V_A, the inertial forces must eventually prevail, regardless of the magnitude of η_E, by overwhelming the viscous resistance to produce fine droplets.

These results complement and expand upon previous work relating the atomization of polymer solutions to elongational viscosity. Fergusson et al. (1992) examined the atomization of aqueous polymer solutions of higher concentration and lower molecular weight, using much lower atomization velocities than those examined here; however, they found similar relationships between atomization behavior and polymer concentration and molecular weight. Fergusson et al. also suggest a relationship between atomization behavior and elongational viscosity, but no direct correlations of the atomization behavior of their solutions with elongational viscosities were made in their study. The study of Chao et al. (1984) does establish a relationship between the antimisting effectiveness of PIB in kerosene solutions and the elongational properties of those solutions, as estimated by a ductless siphon technique (Chao and Williams, 1983). However, that study emphasized measurements of mist ignition energy rather than drop size, and aerosol drop sizes were only evaluated semiquantiatively, by characterizing photographed spray textures according to a numerical scale of 1–5 devised by the authors. Drop size distributions such as those shown in Figures 4–10 were not measured, and consequently quantitative correlations of drop size with rheological parameters were not produced. Also, the ductless siphon method employed by Chao et al. for characterization of elongational viscosity does not permit direct control of the strain rate. Thus elongational flow properties could not be evaluated at the strain rates (or equivalently, the extensional stress values) pertaining to the atomization kinematics, whereas employment of the FENE-P model in this work allows us to characterize the dependence of elongational viscosity on the measured atomization stresses.

The correlation of drop size with η_E shown here offers strong evidence that the atomization behavior of elastic solutions is directly dependent upon the stress-dependent elongational viscosities of these solutions, and that modification of a liquid's elongational viscosity is an effective means for controlling atomization behavior. Like most other investigations of liquid breakup in the atomization regime, the results shown here constitute an empirical correlation, rather than a fluid mechanical model of atomization behavior. However, the strong stabilizing influence of the elastic extensional stresses associated with the high-η_E PIB solutions is apparent, suggesting that these elastic stresses are a very important feature of the breakup mechanism during atomization of viscoelastic liquids. Not withstanding the experimental difficulties of elongational viscosity measurements discussed earlier, the important role of η_E shown here through the predictions of the FENE-P model underscores the need for direct measurements of η_E at strain rates pertaining to atomization.

Conclusions

Atomization studies were conducted on mineral-oil–PIB solutions over a wide range of atomization conditions using a small-scale coaxial flow atomizer. Test solutions covered a range of PIB concentrations and molecular weights, as well as two different oil viscosities. These solutions showed a marked increase in the average aerosol drop size (up to 200%), relative to pure mineral oil, under all atomization conditions, thereby confirming the effectiveness of high molecular weight ($MW > 10^6$) PIB as an antimisting additive for machining oils. The increase in the average drop size of the aerosols, as a result of the PIB additions, varied linearly with the stress-dependent elongational viscosities of these solutions, as predicted by a FENE-P dumbbell model. This correlation shows that the average drop size resulting from the atomization of viscoelastic solutions depends on the elongational viscosity of the solutions, much as the atomization behavior of a Newtonian fluid depends on shear viscosity.

Acknowledgments

The financial support of this work by Ford Motor Company is gratefully acknowledged. The authors also thank Richard S. Marano of Ford Motor Company's Scientific Research Laboratory for his assistance in the industrial application of this research. We are also grateful to Prof. Michael C. Williams for his careful review of the manuscript and his many useful suggestions.

Notation

b = dimensionless FENE parameter
k = Boltzmann constant
M_N = number average molecular weight
M_W = weight average molecular weight
N_A = Avogadro's number
Q_X, Q_Y = component of Q in directions x and y transverse to flow direction
Q_Z = component of Q in direction of flow, z
T = temperature
V = velocity
ρ = density
σ = surface tension
ω = frequency

Subscripts

R = air relative to liquid
L = liquid
atm = atmospheric pressure

Literature Cited

Bechtel, S. E., K. J. Lin, and M. G. Forest, "Effective Stress Rates of Viscoelastic Free Jets," *J. Non-Newtonian Fluid Mech.*, **26**, 1 (1987).

Bird, R. B., R. C. Armstrong, and O. Hassager, *Dynamics of Polymeric Liquids*, Vol. 1, *Fluid Mechanics*, Wiley-Interscience, New York (1987a).

Bird, R. B., C. F. Curtiss, R. C. Armstrong, and O. Hassager, *Dynamics of Polymeric Liquids*, Vol. 2, *Kinetic Theory*, Wiley-Interscience, New York (1987b).

Bousfield, D. W., R. Keunings, G. Marrucci, and M. M. Denn, "Nonlinear Analysis of the Surface Tension Driven Breakup of Viscoelastic Filaments," *J. Non-Newtonian Fluid Mech.*, **21**, 79 (1986).

Chao, K. K., C. A. Child, E. A. Grens, and M. C. Williams, "Anti-misting Action of Polymeric Additives in Jet Fuels," *AIChE J.*, **30**, 111 (1984).

Chao, K. K., and M. C. Williams, "The Ductless Siphon: A Useful Test for Evaluating Dilute Polymer Solution Elongational Behavior. Consistency with Molecular Theory and Parameters," *J. Rheol.*, **27**(5), 451 (1983).

Ferguson, J., N. E. Hudson, and B. C. H. Warren, "The Break-Up of Fluids in an Extensional Flow Field," *J. Non-Newtonian Fluid Mech.*, **44**, 37 (1992).

Goren, S. L., and M. Gottlieb, "Surface-Tension-Driven Breakup of Viscoelastic Liquid Threads," *J. Fluid Mech.*, **120**, 245 (1982).

Hoyt, J. W., J. J. Taylor, and R. L. Altman, "Drag Reduction-Jet Breakup Correlation with Kerosene-Based Additives," *J. Rheol.*, **24**(5), 685 (1980).

Lefebvre, A. H., "Airblast Atomization," *Prog. Energy Combust. Sci.*, **6**, 223 (1980).

Nukiyama, S., and Y. Tanasawa, "Experiments on the Atomization of Liquids in an Air Stream, Report #4: The Influence of the Characteristics of the Liquids on the Diameter of the Atomized Droplets," *Soc. Mech. Eng. Japan*, **5**, 68 (1939).

Peng, S. T. J., and R. F. Landel, "Rheological Behavior of FM-9 Solutions and Correlations with Flammability Test Results and Interpretations," *J. Non-Newtonian Fluid Mech.*, **12**, 95 (1983).

Rizk, N. K., and A. H. Lefebvre, "Spray Characteristics of Plain-Jet Airblast Atomizers," *Trans. ASME, J. Eng. Gas Turbines Power*, **106**, 634 (1984).

Rodriguez, F., *Principle of Polymer Systems*, 3rd ed., Hemisphere, New York (1989).

Smolinski, J. M., "Atomization of Dilute Polyisobutylene/Mineral Oil Solutions," PhD Diss., Wayne State Univ., Detroit, MI (1994).

Sridhar, T., "An Overview of the Project M1," *J. Non-Newtonian Fluid Mech.*, **35**, 85 (1990).

Swithenbank, J., J. M. Beer, D. S. Taylor, and G. C. McCreath, "A Laser Diagnostic Technique for the Measurement of Droplet and Particle Size Distribution," *Prog. Astronaut. Aeronaut.*, **53**, 421 (1977).

Walters, K., "Recent Developments in Rheometry," *Theoretical and Applied Rheology*, P. Moldenaers and R. Keunings, eds., Elsevier, Amsterdam, p. 16 (1992).

Appendix A: Evaluation of Normal Stress Differences Due to Shear Flow

Assuming Poiseuille flow, the liquid flow rate used for testing all oil–PIB solutions, 3.3 mL/min (0.55×10^{-7} m^3/s), corresponds to a shear rate of 420 s^{-1} in the liquid supply tube.

The largest possible normal stress difference due to polymer viscoelasticity will occur with the L-80 solution with c = 1.0 g/L (L-140 has a larger relaxation time than L-80, but it is used at much lower concentrations, yielding a smaller normal stress difference). Using the measured relaxation time from Table B1, $\lambda = 0.00145$ s for L-80 in oil A, we obtain the Weissenberg number (dimensionless shear rate) $\lambda\dot{\gamma} = 0.61$.

For $\lambda\dot{\gamma} < 1$, we do not expect large normal stress effects. This conclusion is easily confirmed by calculating the first normal stress difference N_1 predicted by the Hookean dumbbell kinetic theory for the case of L-80 at 1.0 g/L. The Hookean dumbbell model (Bird et al., 1987b) predicts:

$$N_1 = 2nkT(\lambda\dot{\gamma})^2 \tag{A1}$$

Using $c[\eta]\eta_S = nkT\lambda$, as discussed in Appendix B, we obtain:

$$\begin{aligned} N_1 &= 2c[\eta]\eta_S\dot{\gamma}(\lambda\dot{\gamma}) \\ &= 2(1\text{ kg/m}^3)(0.164\text{ m}^3/\text{kg})(0.02\text{ Pa}\cdot\text{s})(420\text{ s}^{-1})(0.61) \\ &= 1.7\text{ Pa}. \end{aligned} \tag{A2}$$

This value for N_1 is small compared to the prevailing shear stress $\tau_w = (0.02\text{ Pa}\cdot\text{s})(420\text{ s}^{-1}) = 8.4$ Pa, and it is three orders of magnitude smaller than the lowest extensional stress reported in Figure 3. For these reasons, we conclude that normal stress effects due to shear flow in the supply tube are negligible for the purpose of evaluating the extensional stress in Eq. 2.

The Hookean dumbbell model was used in this analysis because of its simplicity. The FENE-P dumbbell model, which accounts for finite extensibility of the chain, would give a somewhat lower value for N_1 than the Hookean dumbbell. Both the Hookean and FENE-P dumbbell models predict $N_2 = 0$ for the second normal stress difference. Experimentally, the second normal stress difference is often found to be nonzero, equal in magnitude to about $N_1/10$. Thus second normal stress effects are also negligible in our development of Eq. 2.

Appendix B: Relaxation Times

The intrinsic viscosity and relaxation time for each of the oil–PIB systems were evaluated, respectively, by measurements of shear viscosity as a function of PIB concentration and of the storage modulus as a function of frequency. Since shear viscosity was found to vary linearly with concentration, intrinsic viscosities could be determined from measurements of steady shear viscosity, at various concentrations for each oil–PIB system, using the following equation:

$$\eta = \eta_S(1 + c[\eta]). \tag{B1}$$

The calculated PIB intrinsic viscosities in oil A (Table B1) appear to depend on molecular weight raised to a power near 0.8, indicating that oil A is a good solvent for PIB. However, the variation of M_W in these experiments encompasses a range much too narrow (1.0–2.2×10^6) to evaluate this scaling exponent with precision. Comparison of measured intrinsic viscosities with corresponding intrinsic viscosities for theta solutions provides additional evidence that oil A is a good solvent; the measured values are consistently greater than the theta-solution values, indicating that the polymer coils are expanded by the solvent.

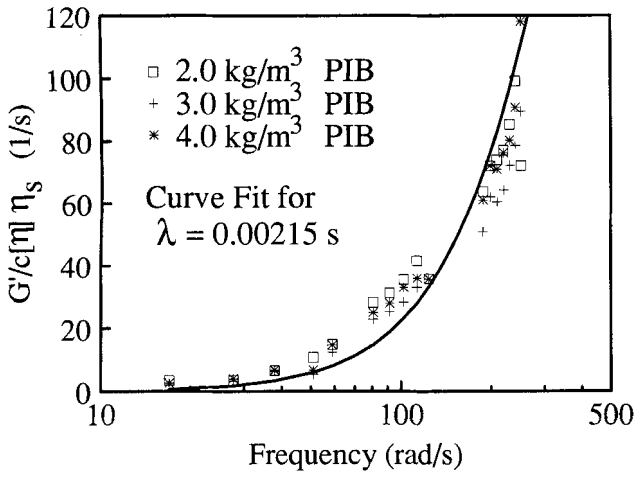

Figure B1. Fit of relaxation time to storage modulus data for L-120 in oil A.

Relaxation times, λ, were evaluated from the storage modulus data by employing the Hookean dumbbell molecular theory (Bird et al., 1987b), which gives

$$G' = nkT\frac{\lambda^2\omega^2}{1+\lambda^2\omega^2}. \tag{B2}$$

Using

$$\eta - \eta_S = c\eta_S[\eta] = nkT\lambda \tag{B3}$$

also predicted by the Hookean dumbbell model, we obtain

$$\frac{G'}{c[\eta]\eta_S} = \frac{\omega^2\lambda}{1+\omega^2\lambda^2}, \tag{B4}$$

giving relaxation time as a function of measured parameters. Equation B4 was selected primarily because of its simplicity. The Hookean dumbbell model oversimplifies several important characteristics of the PIB solutions: the PIB grades are highly polydisperse ($M_W/M_N \approx 2$), whereas the Hookean dumbbells are presumed to be monodisperse; high molecular weight PIB molecules exhibit a spectrum of relaxation times, whereas the model has only a single relaxation time; and the oil is a good solvent for PIB, whereas the Hookean connector force corresponds to Gaussian polymer chain statistics, which prevail only in theta solvents. Nevertheless, the fit of this single relaxation time to the experimental data was rather good

Table B1. Rheological Properties of Oil/PIB Systems

Oil/PIB System	Relaxation Time (s)		$[\eta]$	$[\eta]_\theta$*
	$\lambda_{\text{Oscillatory Testing}}$	$\lambda_{\text{Light Scattering}}$	m^3/kg	m^3/kg
L-80 in oil A	0.00145	0.00119	0.164	0.116
L-80 in oil B	0.00075	—	0.235	0.116
L-100 in oil A	0.00168	0.00147	0.199	0.123
L-120 in oil A	0.00215	0.00166	0.247	0.138
L-140 in oil A	0.00265	0.00194	0.305	0.157

*Calculated for PIB in a theta solvent from M_W values (Table 1) and parameters given in Rodriguez (1989).

Table B2. Value Used in the Estimation of the FENE Parameter b

PIB Grade	$\langle Q_0^2\rangle$ m^2	$\langle r_0^2\rangle_\theta \approx \langle Q_{eq}^2\rangle$ m^2	b
L-80	2.1×10^{-11}	5.7×10^{-15}	11,000
L-100	3.7×10^{-11}	7.6×10^{-15}	14,700
L-120	5.9×10^{-11}	9.5×10^{-15}	18,600
L-140	9.8×10^{-11}	12.3×10^{-15}	23,700

(Figure B1). Relaxation times could also have been evaluated by fitting Eq. B2 to the data directly or from measured intrinsic viscosities using Eq. B3. However, these methods would require evaluation of the number concentration of polymer molecules, n. Direct evaluation of n is complicated by the fact that the PIB grades used here are highly polydisperse, while the Hookean dumbbell model assumes a monodisperse polymer. Also, the GPC molecular weight characterization was interpreted relative to polystyrene standards, and is therefore not absolute. Hence, Eq. B4, which combines Eqs. B2 and B3 to eliminate n, is preferred because this method avoids propagation of the uncertainty in n into the evaluation of λ.

The uncertainties in n do enter into our rheological calculations later in the evaluation of η_E using the FENE-P model, where the use of n is unavoidable. There we employ $n = cN_A/M_W$, where M_W is selected to represent molecular weight because it is more closely associated with the viscosity of polydisperse polymer solutions than M_N. Another related issue that may need clarification is the reconciliation of the use of the Hookean dumbbell model to predict $G'(\omega)$ in Eq. B4 with the use of the FENE-P model for predicting η_E in Eqs. 8–11. These two model predictions are mutually consistent because the FENE-P model reduces to the Hookean dumbbell model in the linear viscoelastic limit, where G' is evaluated, when the parameter b is large, as in the cases evaluated here.

The relaxation times determined for each of the oil/PIB systems are given in Table B1. To confirm the mechanical measurements, the relaxation times for these solutions were also evaluated from the coil diffusion coefficients measured by dynamic light scattering. These two methods yielded relaxation times in good agreement with one another.

Contour Lengths

The FENE parameter b, defined by Eq. 7, requires the estimation of molecular contour length and the equilibrium configuration of an equivalent Hookean polymer chain. Molecular contour lengths were calculated from the weight average molecular weight, as determined by GPC measurements, from which the average number of monomer units per polymer chain was obtained. The length of the monomer unit, ≈ 2.52 Å, was calculated from bond lengths and angles, allowing for the estimation of contour lengths. The equilibrium Hookean chain configurations were approximated by the end-to-end distance of PIB molecules in a theta solvent (Rodriguez, 1989), as given in Table B2.

Manuscript received June 30, 1994, and revision received Aug. 9, 1995.